A Calibration Procedure for Reconfigurable Gough-Stewart Manipulators

Matteo Russo[1], Xin Dong[1]

[1]Department of Mechanical, Materials and Manufacturing Engineering
University of Nottingham, Nottingham, UK
matteo.russo@nottingham.ac.uk

Abstract. This paper introduces a calibration procedure for the identification of the geometrical parameters of a reconfigurable Gough-Stewart parallel manipulator. By using the proposed method, the geometry of a general Gough-Stewart platform can be evaluated through the measurement of the distance between couples of points on the base and mobile platform, repeated for a given set of different poses of the manipulator. The mathematical modelling of the problem is described and a numeric algorithm for an efficient solution to the problem is proposed. Furthermore, an application of the proposed method is discussed with a numerical example, and the behaviour of the calibration procedure is analysed as a function of the number of acquisitions and the number of poses.

Keywords: Calibration; Parallel Manipulators; Gough-Stewart; Hexapod; Robotics; Kinematics.

Nomenclature

Var	Description	Var	Description
$\boldsymbol{B}$	Jacobian matrix of readings wrt pose	o_i	Offset of the i^{th} limb (minimum distance between F_i and M_i)
$\boldsymbol{C}$	Calibration matrix	$\boldsymbol{p}$	Parameter vector to calibrate
e_j	Reading error evaluated as difference between r_j and ρ_j	$\boldsymbol{R}$	Rotation matrix of the mobile platform wrt the base platform
e_{max}	Maximum admitted calibration error	r_j	Distance between S_j and T_j as acquired by the j^{th} sensor
F_i	Centre point of the i^{th} joint on the base platform	$\boldsymbol{r_j}$	Position vector associated to r_j
$\boldsymbol{f_i}$	Absolute position vector of point F_i	S_j	Location of the j^{th} distance sensor on the mobile platform
H	Centre point of the mobile platform	$\boldsymbol{s_i}$	Position vector of point S_i
$\boldsymbol{h}$	Absolute position vector of point H	$\boldsymbol{S}$	Jacobian matrix of limb lengths wrt pose
i	Limb index	T_j	Location of the j^{th} measurement target on the base platform
j	Sensor index	$\boldsymbol{t_i}$	Absolute position vector of point T_i
k	Pose index	$\boldsymbol{u_i}$	Unit vector in the direction of the i^{th} limb
l_i	Stroke of the linear motor of the i^{th} limb	$\boldsymbol{v_j}$	Unit vector in the direction of the j^{th} distance acquisition
$\boldsymbol{l_i}$	Limb vector of the i^{th} limb, from F_i to M_i	x	First position coordinate of point H (along X-axis)
$\boldsymbol{M}$	Jacobian matrix of limb lengths wrt parameters $\boldsymbol{m_j}$ and $\boldsymbol{f_j}$	y	Second position coordinate of point H (along Y-axis)
M_i	Centre point of the i^{th} joint on the mobile platform	z	Third position coordinate of point H (along Z-axis)
$\boldsymbol{m_i}$	Position vector of point F_i in the mobile platform frame	ρ_j	Distance between S_j and T_j as estimated from kinematics
$\boldsymbol{N}$	Jacobian matrix of readings wrt parameters $\boldsymbol{s_j}$ and $\boldsymbol{t_j}$	α	First orientation coordinate of point H (around X-axis)
n_p	Number of poses	β	Second orientation coordinate of point H (around Y-axis)
n_r	Number of sensors	γ	Third orientation coordinate of point H (around Z-axis)

1 Introduction

Parallel robots are closed-loop mechanisms that are characterized by high stiffness, payload capability and repeatability [1]. However, the knowledge of their geometrical parameters is needed to obtain a good accuracy for precision tasks, such as machining. Position control requires the location of the centres of the joints and the offsets of the links. Estimates of these parameters are usually available, but deviations due to manufacturing and assembly tolerances can alter significantly their real values.

Furthermore, the estimation of some parameters might not be available at all. Thus, the identification of the geometry of a parallel robot is essential to its proper functioning.

In his book, Merlet [1] identifies three main calibration methods for parallel kinematic machines: external calibrations, which are based on measurements with external devices; constrained calibrations, which analyse the motion of the robot in a constrained configuration; auto-calibrations, that only rely on the internal sensors of the robot. These methods have been successfully used in the last decades, as proved by the wide literature available [1]. Historically, interest in parallel robot calibration rose in the 1990s with the increasingly common usage of the Gough-Stewart platform in industry [2] and the invention of the Delta Robot [3]. Both self-calibration and external calibration methods can be found: in [4], for example, an implicit-loop method is proposed to calibrate a Gough-Stewart platform with Inverse Kinematics through internal sensors on the spherical and universal joint of one of the parallel limbs; in [5], a constrained calibration is described. Another constrained calibration method is introduced in [6], who proposed a self-calibration of a Gough-Stewart manipulator without external sensors. The same authors also proposed a calibration procedure with two inclinometers in [7]. In [8], a calibration with a redundant leg is presented.

While most of the works of the 1990s are focused on practical calibration methods, in the early 2000s several papers on calibration modelling were published. The research in [9] presents a method to determine all the identifiable parameters of parallel robots, again with a focus on the Gough-Stewart platform. A complete description of the Gough-Steward platform is also given in [10]. The new decade was also characterized by the rise of new technologies, such as vision-based metrology. While most of the methods of the 1990s focus on reducing the number of sensors or simplifying the data acquisition phase, most of the calibration techniques in the 2000s are based either on laser trackers [11-12] or cameras [13-17]. Research on alternative procedures, however, went on, as reported in [18-21]. The most recent works on parallel robot calibration are very wide in scope, with papers on mechanism synthesis and design [22-23], calibration methods [24-25], non-geometric calibration [26], application to innovative designs [27-30] and error models [31-34].

Calibration methods for the Gough-Stewart manipulator usually assume a fixed configuration, where an estimate is available for the parameters and only small errors due to manufacturing and assembly tolerances need to be evaluated. Thus, most of the standard calibration methods fail to converge when some of the parameters are unknown or show a large deviation from the initial estimated value. In [33], an innovative hexapod design is presented as based on the Gough-Stewart architecture with a reconfigurable geometry of the base platform. Since the position of the fixed joints of the machine can change from installation to installation, an onboard calibration procedure with external sensors (three double ball-bars) is manually performed before each operation in order to identify the robot geometry. A further evolution of the design in [33] is described in [34], which introduces a camera-based self-calibration method to identify the position of the fixed joints on the ground. The method is detailed for a three-camera vision system with a previous calibration of the other geometrical parameters through cameras, laser trackers and additional sensors. The calibration methods in [33-34] are tailored for their specific applications, by modelling a Gough-Stewart mechanism with reconfigurable base platform and the specific distance sensor that are selected for the application. Thus, they cannot be used in a general configuration that is characterized by a different kind of distance sensors or by a reconfigurable geometry of the mobile platform (in addition to a reconfigurable fixed platform).

To overcome this limitation, this paper expands the mathematical model introduced in [34] with a general approach for the identification of the geometry of a reconfigurable Gough-Stewart parallel manipulator with no *a-priori* knowledge of the location of any passive joint (including the joints on the mobile platform). The proposed calibration procedure requires distance sensors to measure the distance between a point of the moving platform and a target on the base platform. The calibration problem is defined for a general setup, which does not rely on the kind and number of sensors and can be adapted to a wide range of applications. First, the geometry of the problem is described, and the kinematics of the Gough-Stewart platform are detailed. Then, the algorithm for the geometrical identification is explained. Finally, a numerical example is reported in order to validate the proposed method and to analyse the influence of the calibration parameters on the results.

2 Mechanism description

The Gough-Stewart mechanism, often called *hexapod*, is based on a 6-UPS parallel architecture with six identical limbs of varying length, which are controlled by linear motors. The limbs are connected to the moving platform with universal joints and to the base platform through spherical joints. With reference to Fig. 1, in this paper the following nomenclature is used to describe the geometry of the Gough-Stewart manipulator:

- The location of the centre of the joints on the base platform is defined by point F_i, for i = 1…6, while the corresponding joint on the moving platform is defined by point M_i.
- The position of each joint on the base platform is expressed by position vector $\boldsymbol{f_i}$, while the relative position of each joint on the moving platform with respect to centre point H is expressed by position vector $\boldsymbol{m_i}$.
- The location of point H can be expressed by position vector $\boldsymbol{h}$ $(x\ y\ z)$ and orientation $(\alpha\ \beta\ \gamma)$, by assuming the rotation matrix $\boldsymbol{R}$ of the moving platform being composed by a rotation by γ around the Z-axis first, then by α around the X-axis and finally by β around the Y-axis.
- Each limb is modelled as a rigid link with length equal to the sum of a fixed offset o_i and a variable length controlled by the motor, which is measured by the motor encoder as reading l_i.
- Limb vector $\boldsymbol{l_i}$, going from F_i to M_i, can be written as $(l_i + o_i)\ \boldsymbol{u_i}$, where $\boldsymbol{u_i}$ is a unit vector in the direction of the i^{th} limb.

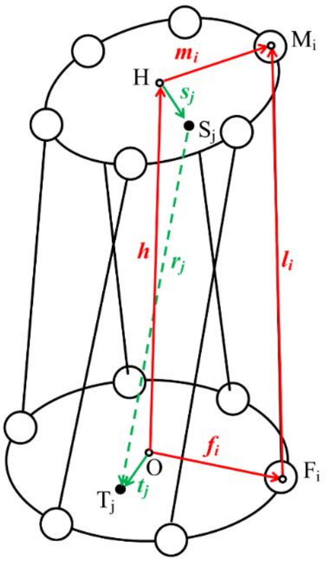

Fig. 1. Kinematic scheme of a Gough-Stewart platform.

With reference to Fig. 1, the following parameters are used to define the geometry of the calibration system:

- The location of the j^{th} distance sensor on the moving platform is defined by point S_j. The corresponding measurement target on the base platform is point T_j.
- The position of each target on the base platform is expressed by position vector $\boldsymbol{t_i}$, while the relative position of each sensor on the moving platform with respect to centre point H is expressed by position vector $\boldsymbol{s_i}$.
- Each sensor can acquire the distance between point S_j and point T_j, which is equal to sensor reading r_j, with an associated reading vector $\boldsymbol{r_j}$, equal to $r_j\ \boldsymbol{v_j}$.
- A total of n_r acquisitions can be obtained for each pose of the Gough-Steward platform. Each acquisition is defined by index j.
- The total number of poses used in a calibration is expressed by n_p, while each pose is defined by index k.

In order to define a calibration procedure, the inverse kinematic problem (IKP) of the hexapod is mathematically defined by writing loop-closure equations for the i^{th} limb as:

$$\boldsymbol{f_i} + \boldsymbol{l_i} = \boldsymbol{h} + \boldsymbol{Rm_i} \tag{2.1}$$

The solution of inverse kinematics requires an expression for the i^{th} limb length as a function of the position of the moving platform, given by $\boldsymbol{h}$ and $\boldsymbol{R}$. Thus, Eq. 2.1 can be rewritten as

$$(o_i + l_i)^2 = (\boldsymbol{h} + \boldsymbol{Rm_i} - \boldsymbol{f_i})^T \cdot (\boldsymbol{h} + \boldsymbol{Rm_i} - \boldsymbol{f_i}) \tag{2.2}$$

When the pose of the moving platform is known, the inverse kinematic formulation can be used to evaluate a theoretical reading for the j^{th} distance sensor. In particular, Eq. 2.2 can be written to express a reading of the j^{th} distance sensor as a function of the pose, as

$$r_j{}^2 = \left(\boldsymbol{h} + \boldsymbol{Rs_j} - \boldsymbol{t_j}\right)^T \cdot \left(\boldsymbol{h} + \boldsymbol{Rs_j} - \boldsymbol{t_j}\right) \tag{2.3}$$

Even if the inverse kinematics of the hexapod are easy to express in closed form, the forward kinematic problem (FKP) leads to multiple solutions and is usually evaluated in a discrete way [1]. In this paper, a simple iterative procedure based on the Newton-Raphson method with the steps in Fig. 2 is used to solve forward kinematics.

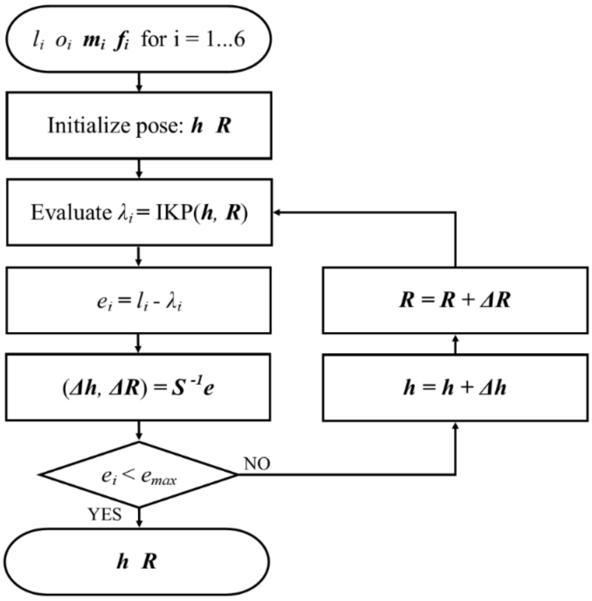

Fig. 2. Algorithm for the solution of forward kinematics.

The inputs for the algorithm in Fig. 2 are the parameters of the manipulator (position of the mobile and fixed joints, offsets of the limbs) and leg displacements. The algorithm starts by defining a tentative pose of the moving platform. With this pose, the inverse kinematic problem is used to evaluate a theoretical limb displacement. The error between the theoretical limb displacement and the input one is evaluated, and a correction of the pose is estimated by using matrix $\boldsymbol{S}$, which is the 6x6 matrix of the partial derivatives of the leg length with respect to the pose, given by

$$\boldsymbol{S} = \begin{bmatrix} \boldsymbol{u}_1^T & \boldsymbol{u}_1^T \cdot \frac{\partial \boldsymbol{R}}{\partial \alpha} \cdot \boldsymbol{m_1} & \boldsymbol{u}_1^T \cdot \frac{\partial \boldsymbol{R}}{\partial \beta} \cdot \boldsymbol{m_1} & \boldsymbol{u}_1^T \cdot \frac{\partial \boldsymbol{R}}{\partial \gamma} \cdot \boldsymbol{m_1} \\ \vdots & \vdots & \vdots & \vdots \\ \boldsymbol{u}_6^T & \boldsymbol{u}_6^T \cdot \frac{\partial \boldsymbol{R}}{\partial \alpha} \cdot \boldsymbol{m_6} & \boldsymbol{u}_6^T \cdot \frac{\partial \boldsymbol{R}}{\partial \beta} \cdot \boldsymbol{m_6} & \boldsymbol{u}_6^T \cdot \frac{\partial \boldsymbol{R}}{\partial \gamma} \cdot \boldsymbol{m_6} \end{bmatrix} \tag{2.4}$$

Matrix $\boldsymbol{S}$ can be used to relate a small displacement in limb length to a small displacement of the pose, as

$$\begin{pmatrix} \Delta l_1 \\ \Delta l_2 \\ \Delta l_3 \\ \Delta l_4 \\ \Delta l_5 \\ \Delta l_6 \end{pmatrix} = \boldsymbol{S} \begin{pmatrix} \Delta x \\ \Delta y \\ \Delta z \\ \Delta \alpha \\ \Delta \beta \\ \Delta \gamma \end{pmatrix} \tag{2.5}$$

and it is used in the algorithm in Fig. 1 as inverse of $\boldsymbol{S}$ to evaluate the pose correction from the error in limb displacement. The derivation of Eq. (2.5) can be found in Appendix A. When the maximum error obtained in the iterative process is lower than the desired accuracy e_{max}, the solution is found.

3 Calibration procedure

This section presents the mathematical modelling of a calibration procedure that identifies the geometry of a reconfigurable Gough-Stewart platform, which is characterized by a variable position of the joints of the fixed and mobile platform, defined by vectors $\boldsymbol{f_i}$ and $\boldsymbol{m_i}$. The calibration is achieved by measuring the distance between points of the moving platform and targets on the base platform, which can be acquired by any kind of distance sensor.

By assuming perfect passive joints, a general Gough-Stewart platform is characterized by 42 identifiable parameters, namely the *xyz* coordinates of the mobile joints (18) and fixed joints (18) and the limb offsets (6). However, *a priori* estimates are available for the full set of parameters. In a reconfigurable platform, *a priori* knowledge can be used only for a small subset of 6 parameters, corresponding to the limb offsets, while the others are unknown. Furthermore, the parameters of the calibration system require identification too. To compensate errors due to sensor positioning and assembly, the *xyz* coordinates of sensors ($3n_r$) and of measurement targets ($3n_r$) can be calibrated, for a total of $6n_r$ additional parameters. Thus, the number of parameters to be calibrated is equal to $42 + 6n_r$ if the offsets are included in the calibration, or to $36 + 6n_r$ for a simplified model that does not include them. For each pose of the moving platform, $6 + n_r$ measurements can be obtained, respectively by the encoders of the linear motors and the distance sensors. By acquiring data in n_p different poses, it is possible to increase the number of samples available, thus improving the calibration results. The constraint functions derive from the kinematic model of the robot in Eqs. 2.1-3, and relate the acquired measurements to the calibrated parameters. In particular, for a given pose k, a theoretical reading ρ of the j^{th} sensor can be evaluated as a function of the pose by using Eq. 2.3 as

$$\rho_{j,k}{}^2 = \left(\boldsymbol{h_k} + \boldsymbol{R_k}\boldsymbol{s_j} - \boldsymbol{t_j}\right)^T \cdot \left(\boldsymbol{h_k} + \boldsymbol{R_k}\boldsymbol{s_j} - \boldsymbol{t_j}\right) \tag{3.1}$$

This theoretical value can be compared to the real one, which is acquired through the j^{th} sensor in pose k, to obtain error e, which is defined as

$$e_{j,k} = r_{j,k} - \rho_{j,k} \tag{3.2}$$

In order to calibrate the robot, the influence of both pose and calibration parameters on the reading must be studied by differentiating Eq. 3.1. With an approach similar to the FKP solution one in the previous section, matrix $\boldsymbol{B_{j,k}}$ can be defined as the matrix of the partial derivatives of the reading with respect to the pose, and matrix $\boldsymbol{N_{j,k}}$ as the matrix of the partial derivatives of the reading with respect to parameters $\boldsymbol{s_j}$ and $\boldsymbol{t_j}$. In particular, matrix $\boldsymbol{B_{j,k}}$ is a 1x6 matrix that expresses the following relation:

$$\Delta r_{j,k} = \boldsymbol{B_{j,k}} \begin{pmatrix} \Delta x_k \\ \Delta y_k \\ \Delta z_k \\ \Delta \alpha_k \\ \Delta \beta_k \\ \Delta \gamma_k \end{pmatrix} \tag{3.3}$$

By differentiating Eq. 3.1, $\boldsymbol{B_{j,k}}$ is obtained as a 1x6 matrix given by

$$\boldsymbol{B_{j,k}} = \begin{bmatrix} \boldsymbol{v_{j,k}^T} & \boldsymbol{v_{j,k}^T} \cdot \dfrac{\partial \boldsymbol{R_k}}{\partial \alpha} \cdot \boldsymbol{m_j} & \boldsymbol{v_{j,k}^T} \cdot \dfrac{\partial \boldsymbol{R_k}}{\partial \beta} \cdot \boldsymbol{m_j} & \boldsymbol{v_{j,k}^T} \cdot \dfrac{\partial \boldsymbol{R_k}}{\partial \gamma} \cdot \boldsymbol{m_j} \end{bmatrix} \tag{3.4}$$

Matrix $\boldsymbol{N_{j,k}}$ expresses the following relation:

$$\Delta r_{j,k} = \boldsymbol{N_{j,k}} \begin{pmatrix} \Delta \boldsymbol{t_j} \\ \Delta \boldsymbol{s_j} \end{pmatrix} \tag{3.5}$$

By differentiating Eq. 3.1, $\boldsymbol{N_{j,k}}$ is obtained as a 1x6 matrix given by

$$\boldsymbol{N_{j,k}} = \begin{bmatrix} \boldsymbol{v_{j,k}^T} & -\boldsymbol{v_{j,k}^T}\boldsymbol{R_k} \end{bmatrix} \tag{3.6}$$

Equations 3.3-6 established a relation between a small variation of the reading of a sensor and a small variation in pose and calibration parameters. However, to perform a full calibration, the relation between the pose and the robot parameters must be defined. By using inverse kinematics, it is possible to evaluate matrix $\boldsymbol{S}$ of Eq. 2.4 for the current pose and reading, to express

$$\begin{pmatrix} \Delta l_{1,k} \\ \Delta l_{2,k} \\ \Delta l_{3,k} \\ \Delta l_{4,k} \\ \Delta l_{5,k} \\ \Delta l_{6,k} \end{pmatrix} = \boldsymbol{S_{j,k}} \begin{pmatrix} \Delta x_k \\ \Delta y_k \\ \Delta z_k \\ \Delta \alpha_k \\ \Delta \beta_k \\ \Delta \gamma_k \end{pmatrix} \tag{3.7}$$

where $\boldsymbol{S_{j,k}}$ is a 6x6 matrix given by

$$\boldsymbol{S_{j,k}} = \begin{bmatrix} \boldsymbol{u_{1,k}^T} & \boldsymbol{u_{1,k}^T} \cdot \frac{\partial \boldsymbol{R_k}}{\partial \alpha} \cdot (\boldsymbol{m_1} - \boldsymbol{m_j}) & \boldsymbol{u_1^T} \cdot \frac{\partial \boldsymbol{R_k}}{\partial \beta} \cdot (\boldsymbol{m_1} - \boldsymbol{m_j}) & \boldsymbol{u_1^T} \cdot \frac{\partial \boldsymbol{R_k}}{\partial \gamma} \cdot (\boldsymbol{m_1} - \boldsymbol{m_j}) \\ \vdots & \vdots & \vdots & \vdots \\ \boldsymbol{u_{6,k}^T} & \boldsymbol{u_{6,k}^T} \cdot \frac{\partial \boldsymbol{R_k}}{\partial \alpha} \cdot (\boldsymbol{m_6} - \boldsymbol{m_j}) & \boldsymbol{u_6^T} \cdot \frac{\partial \boldsymbol{R_k}}{\partial \beta} \cdot (\boldsymbol{m_6} - \boldsymbol{m_j}) & \boldsymbol{u_6^T} \cdot \frac{\partial \boldsymbol{R_k}}{\partial \gamma} \cdot (\boldsymbol{m_6} - \boldsymbol{m_j}) \end{bmatrix} \tag{3.8}$$

As explained in Appendix A, matrix $\boldsymbol{M_k}$ is derived from Eq. (2.2) as the 6x36 matrix of the partial derivatives of the limb lengths with respect to parameters $\boldsymbol{m_j}$ and $\boldsymbol{f_j}$, which expresses

$$\begin{pmatrix} \Delta l_{1,k} \\ \Delta l_{2,k} \\ \Delta l_{3,k} \\ \Delta l_{4,k} \\ \Delta l_{5,k} \\ \Delta l_{6,k} \end{pmatrix} = \boldsymbol{M_k} \begin{pmatrix} \Delta \boldsymbol{f_1} \\ \Delta \boldsymbol{m_1} \\ \vdots \\ \Delta \boldsymbol{f_6} \\ \Delta \boldsymbol{m_6} \end{pmatrix} \tag{3.9}$$

and is given by

$$\boldsymbol{M_k} = \begin{bmatrix} \boldsymbol{M_{1,k}} & \boldsymbol{0} & \boldsymbol{0} \\ \boldsymbol{0} & \ddots & \boldsymbol{0} \\ \boldsymbol{0} & \boldsymbol{0} & \boldsymbol{M_{6,k}} \end{bmatrix} \; with \; \boldsymbol{M_{i,k}} = \begin{bmatrix} \boldsymbol{u_{1,k}^T} & -\boldsymbol{u_{1,k}^T} \boldsymbol{R_k} \end{bmatrix} \tag{3.10}$$

By substituting Eq. 3.9 in Eq. 3.7, and then the results in Eq. 3.3, a linearized relation between the reading and the parameters can be written as

$$\Delta r_{j,k} = \begin{bmatrix} (\boldsymbol{B_{j,k}} \cdot \boldsymbol{S_{j,k}^{-1}} \cdot \boldsymbol{M_k}) & \boldsymbol{N_{j,k}} \end{bmatrix} \begin{pmatrix} \Delta \boldsymbol{f_1} \\ \Delta \boldsymbol{m_1} \\ \vdots \\ \Delta \boldsymbol{f_6} \\ \Delta \boldsymbol{m_6} \\ \Delta \boldsymbol{t_j} \\ \Delta \boldsymbol{s_j} \end{pmatrix} \tag{3.11}$$

Equation 3.11 can be expressed in a compact form as

$$\Delta r_{j,k} = \boldsymbol{C_{j,k}} \Delta \boldsymbol{p_j} \tag{3.12}$$

where $\boldsymbol{C_{j,k}}$ is the 1x42 calibration matrix relative to the j^{th} measurement in the k^{th} pose, and $\boldsymbol{\Delta p_j}$ is a reduced parameter vector, with the robot parameters and the calibration parameters relative to the j^{th} measurement only. By using Eq. 3.12, it is possible to compute a correction in the robot parameters due to a reading error as in Eq. 3.2. This error can be minimized through an iterative procedure, as in Fig. 3, to identify the value of parameters to be calibrated.

The procedure described in Fig. 3 is characterized by the acquisition of a single measurement r_j for each pose of the robot. For the iterative process to converge, however, the number of constrain function must be greater than the number of parameters we want to calibrate. Since for each measurement in each pose a single constrain function can be written, as shown in Eq. 3.12, the number of constraint functions is equal to $n_r \cdot n_p$, while the number of parameters is equal to 36 + 6n_r. Therefore, the number of poses and sensors must be chosen to satisfy

$$n_r(n_p - 6) > 36 \tag{3.13}$$

In addition to this, the larger n_r and n_p are, the faster the algorithm converges. Therefore, a system with multiple sensors can be calibrated in a more efficient way.

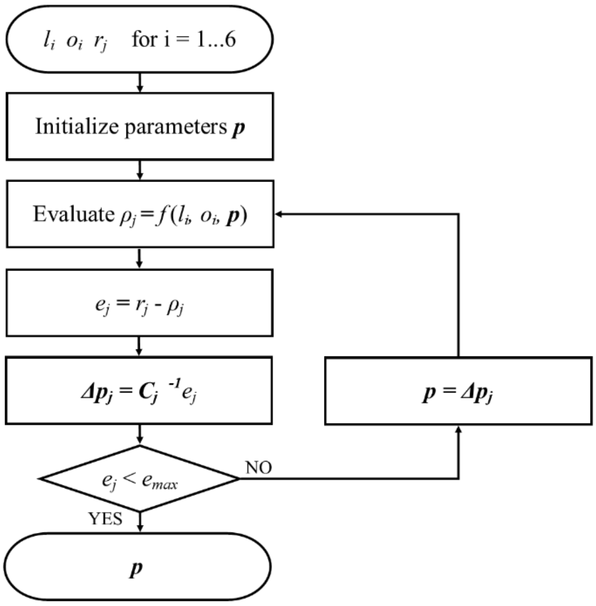

Fig. 3. Algorithm for the identification of the parameters to calibrate.

Thus, the problem formulation introduced in this section for the j^{th} sensor can be expanded for a general number of acquisitions. First of all, Eq. 3.5 can be rewritten as

$$e_{j,k} = \begin{bmatrix} \mathbf{0}_{1\times 6} & \cdots & \boldsymbol{N}_{j,k} & \cdots & \mathbf{0}_{1\times 6} \end{bmatrix} \begin{pmatrix} \Delta\boldsymbol{t}_1 \\ \Delta\boldsymbol{s}_1 \\ \vdots \\ \Delta\boldsymbol{t}_j \\ \Delta\boldsymbol{s}_j \\ \vdots \\ \Delta\boldsymbol{t}_{n_r} \\ \Delta\boldsymbol{s}_{n_r} \end{pmatrix} = \boldsymbol{N}^{\star}_{j,k} \Delta\boldsymbol{p}_{sensors} \tag{3.14}$$

to include a general number of sensors. A variation of the reading of the j^{th} sensor can still be related only to a variation of corresponding points T_j and S_j, but the expanded matrix of Eq. 3.14 can be used to assemble a calibration matrix for pose k by rewriting Eq. 3.12 as

$$\boldsymbol{e}_k = \begin{pmatrix} e_{1,k} \\ \vdots \\ e_{n_r,k} \end{pmatrix} = \begin{bmatrix} \left(\boldsymbol{B}_{1,k} \cdot \boldsymbol{S}^{-1}_{1,k} \cdot \boldsymbol{M}_k\right) & \boldsymbol{N}^{\star}_{1,k} \\ \vdots & \vdots \\ \left(\boldsymbol{B}_{n_r,k} \cdot \boldsymbol{S}^{-1}_{n_r,k} \cdot \boldsymbol{M}_k\right) & \boldsymbol{N}^{\star}_{n_r,k} \end{bmatrix} \begin{pmatrix} \Delta\boldsymbol{f}_1 \\ \Delta\boldsymbol{m}_1 \\ \vdots \\ \Delta\boldsymbol{f}_6 \\ \Delta\boldsymbol{m}_6 \\ \Delta\boldsymbol{t}_1 \\ \Delta\boldsymbol{s}_1 \\ \vdots \\ \Delta\boldsymbol{t}_{n_r} \\ \Delta\boldsymbol{s}_{n_r} \end{pmatrix} = \boldsymbol{C}_k \Delta\boldsymbol{p} \tag{3.15}$$

where $\boldsymbol{e}_k$ is a vector that collects the error of all the acquisitions in pose k, and $\boldsymbol{C}_k$ is the relative n_rx(36+6n_r) calibration matrix, which is assembled from matrices $\boldsymbol{C}_{j,k}$. Equation 3.15 can be then expanded to a general number of poses, as

$$\boldsymbol{e} = \begin{pmatrix} \boldsymbol{e}_1 \\ \vdots \\ \boldsymbol{e}_{n_p} \end{pmatrix} = \begin{bmatrix} \boldsymbol{C}_1 \\ \vdots \\ \boldsymbol{C}_{n_p} \end{bmatrix} \Delta\boldsymbol{p} = \boldsymbol{C}\Delta\boldsymbol{p} \tag{3.16}$$

where $\boldsymbol{e}$ is a vector that collects the error of each acquisition in each pose, and $\boldsymbol{C}$ is the relative ($n_p \cdot n_r$)x(36+6n_r) calibration matrix. In conclusion, the calibration problem can be stated as an optimization problem to find the minimum of the error function $\boldsymbol{e}$ of Eq. 3.15, which is solved by following the procedure outlined in Fig. 3.

4 Calibration in unknown environments

The previous section assumes a known coordinate system for the identification of the position of the joints of the base platform. However, when a reconfigurable hexapod is set up in an unknown environment, it is possible to have no known external geometrical feature to define a coordinate system. Nevertheless, a convention can be established to calibrate the system even in absence of external references. An XYZ frame can be defined by constraining 6 degrees of freedom of the reconfigurable foot joints. These degrees of freedom can be:

- X position of base platform joint F_i;
- Y position of base platform joint F_i;
- Z position of base platform joint F_i;
- Y position of another base platform joint F_j ($i \neq j$);
- Z position of another base platform joint F_j ($i \neq j$);
- Z position of a third base platform joint F_k ($i \neq z$; $j \neq z$);

As illustrated in Fig. 4, when the value of all the fixed degrees of freedom is set to 0, it is possible to summarize the conditions as:

- Origin of the reference coordinate frame in point F_i;
- X-axis passing through points F_i and F_j;
- Z-axis passing through point F_i;
- Z-axis direction perpendicular to the plane defined by F_i, F_j and F_k;
- Y-axis passing through point F_i;
- Y-axis direction perpendicular to the plane defined by X-axis and Z-axis;
- Right hand rule for axis orientation.

By using this guideline, it is possible to univocally define a reference coordinate system to calibrate a Gough-Stewart mechanism even in an unknown environment. This reference system can then be used to calibrate and identify the geometry of the fixed base and the position of the measuring targets.

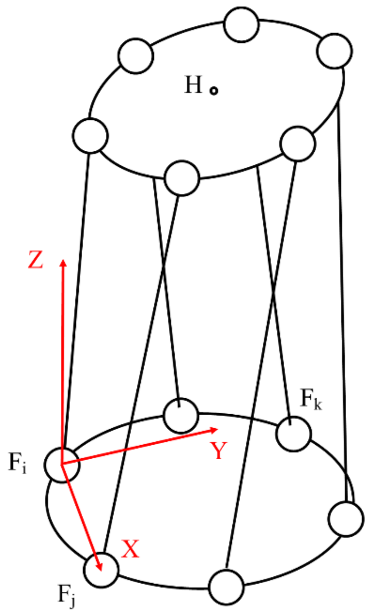

Fig. 4. Definition of a reference coordinate system.

5 Experimental validation

In this section, the proposed calibration procedure is applied to the Free-Hex robot, a reconfigurable Gough-Stewart machining tool, in order to identify the position of its passive joints. Free-Hex, as explained in [33], is a parallel machine tool that is characterized by a mobile platform with fixed geometry and a reconfigurable base platform, with loose magnetic feet at the end of each limb. Since the magnetic feet are positioned before any machining operation in an unknown configuration, a full calibration of the system is needed for proper functioning. A prototype of Free-Hex is shown in Fig. 5. The best available measurement of the geometry of the system, in Table 1, has been used as reference to validate and evaluate the proposed procedure. The reference geometry has been identified through previous external calibrations with a combination of double-ball bars (1μm accuracy) and laser trackers (25μm accuracy), and it is here used as a reference to evaluate the performance of the proposed procedure. The manipulator is equipped with encoders for the linear motors and three double ball-bars as distance sensors, as shown in Fig. 6, that acquire data over 240 calibration poses. To enable the comparison of the proposed calibration to the reference geometry, the reference coordinate frame has been defined through the calibration frame as shown in Fig. 6 and explained in [33]. The initial geometry for the iterative solution estimates the values of all the parameters, as shown in Table 2.

Table 1. Reference geometry for the numerical example.

Point	X [mm]	Y [mm]	Z [mm]	Point	X [mm]	Y [mm]	Z [mm]
F_1	-120.470	-71.189	28.396	M_1	-20.607	-92.760	212.680
F_2	-175.001	50.055	27.435	M_2	-90.611	28.564	212.656
F_3	-11.976	165.859	28.634	M_3	-70.064	64.182	212.664
F_4	123.013	127.391	28.980	M_4	70.047	64.136	212.693
F_5	143.868	-51.709	29.528	M_5	90.599	28.546	212.685
F_6	52.025	-155.265	29.146	M_6	20.525	-92.762	212.683
T_1	0.010	-79.863	15.877	S_1	0.000	-40.006	121.436
T_2	-69.142	39.814	16.147	S_2	-34.646	20.003	121.896
T_3	69.097	39.869	16.014	S_3	34.718	20.016	121.835

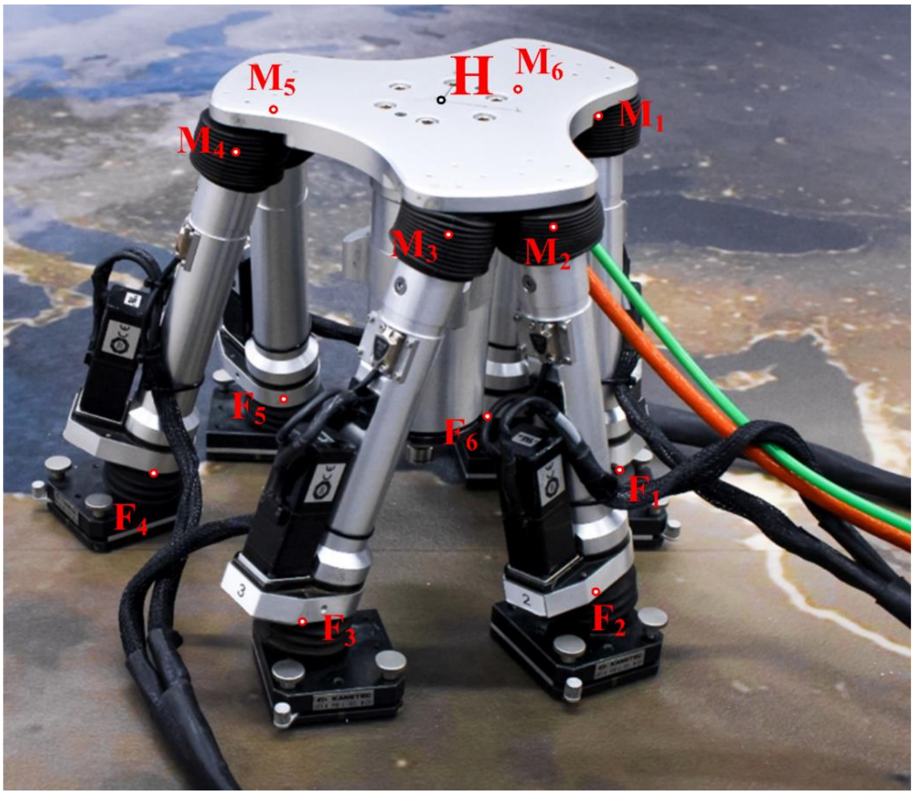

Fig. 5. Free-Hex robot prototype.

Fig. 6. Frame and double ball-bars for the calibration of Free-Hex.

The calibration procedure for the reported test acquires data from 241 calibration poses, generated by recording the initial pose (1 pose), then extending and contracting each linear motor over 10 different steps while all the other motors are fixed (20 poses per motor, 120 poses in total), and finally repeating the entire sequence a second time (120 poses). More than 15 different calibration tests were successfully run, and one of them is here reported as example.

A first partial calibration has been performed by including the location of the passive joints of the base platform as parameters. The procedure converges to a solution in 15 iterations and 23 sec (running the calibration code in MATLAB on a high-spec laptop), as shown in Fig. 7a, with a tolerance on $\boldsymbol{\Delta p}$ equal to 10^{-6} mm and a maximum estimated error equal to 0.015 mm. The results are shown in Table 3. When compared to the reference geometry of Table 1, the average correction is 0.70 mm, with an average relative correction of 0.42% and a maximum relative correction of 0.50%. These values have been calculated as the mean of the norm of the position vector error of each calibrated point.

A second partial calibration has been performed by including the location of all the passive joints as parameters. The procedure converges to a solution in 47 iterations and 29 sec, as reported in Fig. 7b, with a tolerance on $\boldsymbol{\Delta p}$ equal to 10^{-6} mm and a maximum estimated error equal to 0.013 mm. The results are shown in Table 4. When compared to the reference geometry of Table 1, the average correction is equal to 1.94 mm, with an average relative correction of 1.03% and a maximum relative correction of 1.63%.

Finally, a full calibration has been performed to identify both robot geometry and calibration parameters (sensor positioning). The procedure converges to a solution in 75 iterations and 35 sec with convergence in 35 sec and results in Table 5. When compared to the reference geometry of Table 1, the average correction is equal to 1.92 mm, with an average relative correction of 1.04%. Even if the average values are comparable to the partial tests, the maximum relative correction is higher at 2.81%.

The second calibration script has been also run for 100 different initial conditions, characterized by a different layout of the passive joints with a maximum displacement from the reference geometry of 200 mm. The procedure always converges to the same solution, unless two or more joints start from an identical position, for which the forward kinematic solver fails. The maximum number of iterations to convergence observed for the example is 90. Furthermore, the calibration procedure has been tested with a subset of poses as input, in order to evaluate the influence of n_p on calibration quality. A smaller number of poses does not increase the number of iterations to convergence, with 30 to 90 iterations needed for convergence with different subsets. However, divergence issues have been observed for subsets with less than 90 poses. Furthermore, the mean and maximum error with respect to the reference geometry of Table 1 is larger for a smaller number of poses, as reported in Fig. 8. The trend, however, is not linear, with some subsets performing better than others despite having a smaller number of poses. Thus, as a general guideline, a larger set of poses yields better results, but it is possible to observe a sensitivity to which poses are selected, and not only to their number. Therefore, the calibration motion should be optimized for the manipulator under analysis by choosing relevant poses.

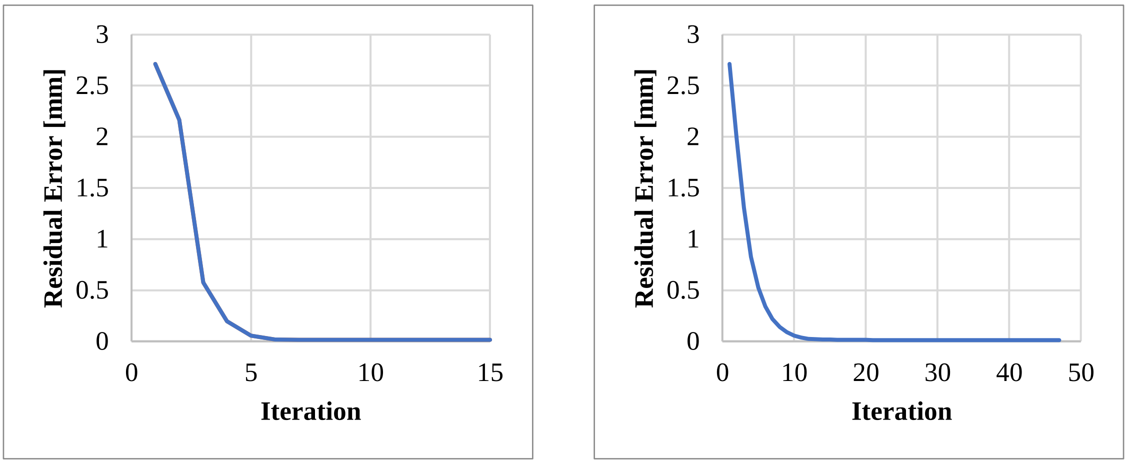

Fig. 7. Convergence graph of the calibration algorithm: a) first calibration (18 parameters, fixed joints); b) second calibration (36 parameters, fixed and mobile joints)

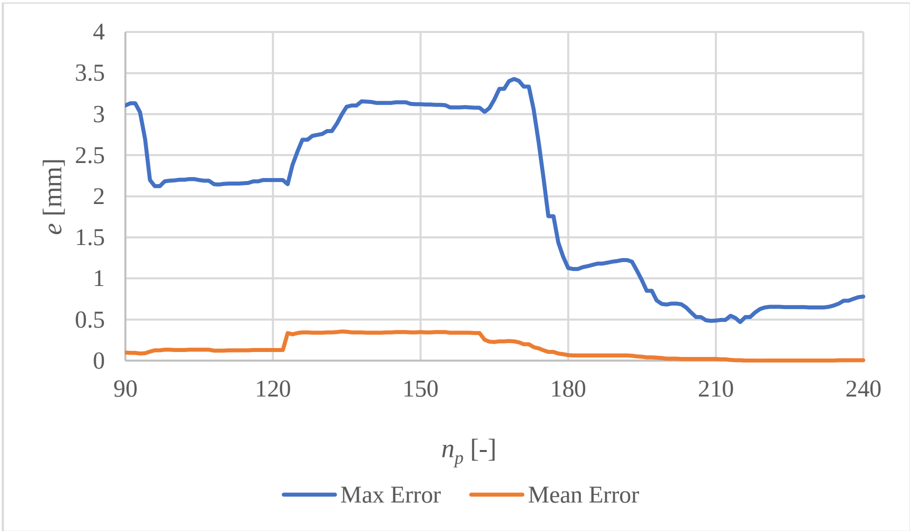

Fig. 8. Influence of number of poses on mean and maximum error.

Table 2. Initial geometry for the calibration procedure.

Point	X [mm]	Y [mm]	Z [mm]	Point	X [mm]	Y [mm]	Z [mm]
F_1	-105.2505	-88.479	0.000	M_1	-20.607	-92.760	212.680
F_2	-129.2505	-46.910	0.000	M_2	-90.611	28.564	212.656
F_3	-24.000	135.3893	0.000	M_3	-70.064	64.182	212.664
F_4	24.000	135.3893	0.000	M_4	70.047	64.136	212.693
F_5	129.2505	-46.910	0.000	M_5	90.599	28.546	212.685
F_6	105.2505	-88.479	0.000	M_6	20.525	-92.762	212.683
T_1	0.010	-79.863	15.877	S_1	0.000	-40.006	121.436
T_2	-69.142	39.814	16.147	S_2	-34.646	20.003	121.896
T_3	69.097	39.869	16.014	S_3	34.718	20.016	121.835

Table 3. Results of the first calibration (18 parameters, fixed joints).

Point	X [mm]	Y [mm]	Z [mm]	Point	X [mm]	Y [mm]	Z [mm]
F_1	-120.029	-71.235	28.889	M_1	-20.607	-92.760	212.680
F_2	-174.696	49.790	28.213	M_2	-90.611	28.564	212.656
F_3	-11.447	165.322	28.470	M_3	-70.064	64.182	212.664
F_4	123.188	127.433	28.228	M_4	70.047	64.136	212.693
F_5	143.872	-51.736	28.749	M_5	90.599	28.546	212.685
F_6	52.132	-155.129	28.863	M_6	20.525	-92.762	212.683
T_1	0.010	-79.863	15.877	S_1	0.000	-40.006	121.436
T_2	-69.142	39.814	16.147	S_2	-34.646	20.003	121.896
T_3	69.097	39.869	16.014	S_3	34.718	20.016	121.835

Table 4. Results of the second calibration (36 parameters, fixed and mobile joints).

Point	X [mm]	Y [mm]	Z [mm]	Point	X [mm]	Y [mm]	Z [mm]
F_1	-119.904	-72.276	27.501	M_1	-19.372	-92.985	212.449
F_2	-176.916	47.949	27.440	M_2	-90.772	27.273	212.640
F_3	-13.767	165.013	28.798	M_3	-71.226	62.709	213.867
F_4	122.748	129.756	28.477	M_4	69.609	65.254	213.066
F_5	144.640	-50.000	27.809	M_5	90.514	30.207	213.272
F_6	54.256	-155.611	28.110	M_6	22.083	-92.131	212.713
T_1	0.010	-79.863	15.877	S_1	0.000	-40.006	121.436
T_2	-69.142	39.814	16.147	S_2	-34.646	20.003	121.896
T_3	69.097	39.869	16.014	S_3	34.718	20.016	121.835

Table 5. Results of the third calibration (54 parameters, fixed and mobile joints, sensors).

Point	X [mm]	Y [mm]	Z [mm]	Point	X [mm]	Y [mm]	Z [mm]
F_1	-119.416	-72.726	26.896	M_1	-18.798	-94.586	210.974
F_2	-176.416	47.651	28.977	M_2	-90.109	25.752	213.334
F_3	-13.020	165.271	31.369	M_3	-70.336	61.596	215.210
F_4	122.791	129.868	29.170	M_4	70.169	64.043	213.420
F_5	144.648	-50.399	25.424	M_5	90.916	28.549	211.778
F_6	54.111	-156.338	25.174	M_6	22.325	-94.007	211.074
T_1	0.053	-79.813	15.863	S_1	-0.126	-40.138	121.375
T_2	-69.123	39.808	16.183	S_2	-34.633	20.050	121.927
T_3	69.109	39.824	15.989	S_3	34.686	20.036	121.867

6 Conclusions

This paper proposed a numeric calibration method for reconfigurable Gough-Stewart manipulators that are characterized by a variable geometry of base and moving platforms. The calibration algorithm expands previous models with a general approach for the geometrical identification with no a-priori knowledge of the location of any passive joint (including the joints on the mobile platform), by using three or more distance measurements from the base to the moving platform acquired for several different poses. The proposed approach is introduced with its mathematical formulation in a general form to be independent from the kind and number of sensors. A convention for the definition of a reference coordinate system is presented in case of unknown external environment. Finally, a numerical example on a reconfigurable Gough-Stewart platform is reported. The tests validate the proposed algorithm with calibration results that are comparable to the reference values, with an average correction of 0.42% for 18 calibration parameters, 1.03% for 36 parameters and 1.04% for 54 parameters.

Acknowledgements

This work was supported by UK EPSRC projects RAIN (grant EP/R026084/1) and Through-life performance: From science to instrumentation (grant EP/P027121/1), and by the Erasmus+ programme of the European Union.

Appendix A

The derivative with respect to time of Eq. (2.2) can be written as

$$\frac{\partial}{\partial t}(o_i + l_i)^2 = \frac{\partial}{\partial t}[(\boldsymbol{h} + \boldsymbol{R}\boldsymbol{m_i} - \boldsymbol{f_i})^T \cdot (\boldsymbol{h} + \boldsymbol{R}\boldsymbol{m_i} - \boldsymbol{f_i})] \tag{A.1}$$

Expanding this equation, it is possible to obtain

$$2l_i\dot{l}_i = 2(\boldsymbol{h} + \boldsymbol{R}\boldsymbol{m_i} - \boldsymbol{f_i})^T \cdot \left[\frac{\partial}{\partial t}(\boldsymbol{h} + \boldsymbol{R}\boldsymbol{m_i} - \boldsymbol{f_i})\right] \tag{A.2}$$

$$2l_i\dot{l}_i = 2(\boldsymbol{h} + \boldsymbol{R}\boldsymbol{m_i} - \boldsymbol{f_i})^T \left[\frac{\partial \boldsymbol{h}}{\partial t} + \frac{\partial \boldsymbol{R}}{\partial t}\boldsymbol{m_i} + \boldsymbol{R}\frac{\partial \boldsymbol{m_i}}{\partial t} - \frac{\partial \boldsymbol{f_i}}{\partial t}\right] \tag{A.3}$$

The limb unit vector can be defined as

$$\boldsymbol{u_i^T} = \frac{\boldsymbol{l_i}}{l_i} = \frac{(\boldsymbol{h} + \boldsymbol{R}\boldsymbol{m_i} - \boldsymbol{f_i})^T}{l_i} \tag{A.4}$$

Thus, Eq. (A.3) can be expressed as

$$\dot{l}_i = \boldsymbol{u_i^T}\left[\frac{\partial \boldsymbol{h}}{\partial t} + \frac{\partial \boldsymbol{R}}{\partial t}\boldsymbol{m_i} + \boldsymbol{R}\frac{\partial \boldsymbol{m_i}}{\partial t} - \frac{\partial \boldsymbol{f_i}}{\partial t}\right] \tag{A.5}$$

In order to derive Eq. (2.5), it is assumed that the geometry of the robot does not change during motion. This condition is expressed by

$$\frac{\partial \boldsymbol{m_i}}{\partial t} = \boldsymbol{0};\ \frac{\partial \boldsymbol{f_i}}{\partial t} = \boldsymbol{0} \tag{A.6}$$

When condition (A.6) is applied to (A.5), Eq. (A.5) becomes

$$\dot{l}_i = \boldsymbol{u_i^T}\left[\frac{\partial \boldsymbol{h}}{\partial t} + \frac{\partial \boldsymbol{R}}{\partial t}\boldsymbol{m_i}\right] \tag{A.7}$$

Equation (A.7) can be expanded as

$$\dot{l}_i = \boldsymbol{u_i^T}\left[\frac{\partial \boldsymbol{h}}{\partial x}\dot{x} + \frac{\partial \boldsymbol{h}}{\partial y}\dot{y} + \frac{\partial \boldsymbol{h}}{\partial z}\dot{z} + \left(\frac{\partial \boldsymbol{R}}{\partial \alpha}\dot{\alpha} + \frac{\partial \boldsymbol{R}}{\partial \beta}\dot{\beta} + \frac{\partial \boldsymbol{R}}{\partial \gamma}\dot{\gamma}\right)\boldsymbol{m_i}\right] \tag{A.8}$$

When Eq. (A.8) is written for limbs 1 to 6, it leads to the virtual displacement notation expressed by Eqs. (2.4) and (2.5).

It is possible to obtain Eq. (3.9) by applying a different condition to Eq. (A.5). In order to estimate the variation of limb lengths from a variation of geometrical parameters, it is possible to assume a fixed pose of the robot. This assumption is given by

$$\frac{\partial \boldsymbol{h}}{\partial t} = \boldsymbol{0};\frac{\partial \boldsymbol{R}}{\partial t} = \boldsymbol{0} \tag{A.9}$$

Thus, Eq. (A.5) can be rewritten for the given case as

$$\Delta l_i = \boldsymbol{u_i^T}[\Delta \boldsymbol{f_i} - \boldsymbol{R}\Delta \boldsymbol{m_i}], \tag{A.10}$$

which leads to Eq. (3.9).

Since the procedure follows a linear approximation with the assumption of small parameter variation, it is possible to study the dependency of limb length on position and geometry independently. The resulting pose error is then obtained as a combination of the two, as expressed in (3.11). A direct derivation of the total differential of Eq. (2.2) yields the same result without decoupling the system and can be obtained by expanding Eq. (A.5) without applying conditions (A.6) or (A.9).

References

1. Merlet, J. P. (2006). *Parallel robots* (Vol. 128). Springer Science & Business Media.
2. Zhuang, H. (1997). Self-calibration of parallel mechanisms with a case study on Stewart platforms. IEEE Transactions on Robotics and Automation, 13(3), 387-397.

3. Vischer, P., & Clavel, R. (1998). Kinematic calibration of the parallel Delta robot. *Robotica*, 16(2), 207-218.
4. Wampler, C. W., Hollerbach, J. M., & Arai, T. (1995). An implicit loop method for kinematic calibration and its application to closed-chain mechanisms. *IEEE Transactions on Robotics and Automation*, 11(5), 710-724.
5. Rauf, A., & Ryu, J. (2001). Fully autonomous calibration of parallel manipulators by imposing position constraint. *In Robotics and Automation, 2001. Proceedings 2001 ICRA. IEEE International Conference on* (Vol. 3, pp. 2389-2394). IEEE.
6. Khalil, W., & Besnard, S. (1999). Self-calibration of Stewart-Gough parallel robots without extra sensors. *IEEE Transactions on Robotics and Automation*, 15(6), 1116-1121.
7. Besnard, S., & Khalil, W. (1999). Calibration of parallel robots using two inclinometers. *In Robotics and Automation, 1999. Proceedings. 1999 IEEE International Conference on* (Vol. 3, pp. 1758-1763). IEEE.
8. Patel, A. J., & Ehmann, K. F. (2000). Calibration of a hexapod machine tool using a redundant leg. *International Journal of Machine Tools and Manufacture*, 40(4), 489-512.
9. Besnard, S., & Khalil, W. (2001). Identifiable parameters for parallel robots kinematic calibration. *In Robotics and Automation, 2001. Proceedings 2001 ICRA. IEEE International Conference on* (Vol. 3, pp. 2859-2866). IEEE.
10. Daney, D. (2003). Kinematic calibration of the Gough platform. *Robotica*, 21(6), 677-690.
11. Yu, D., & Han, J. (2005, July). Kinematic calibration of parallel robots. *In Mechatronics and Automation, 2005 IEEE International Conference* (Vol. 1, pp. 521-525). IEEE.
12. Corbel, D., Nabat, V., & Maurine, P. (2006, August). Geometrical calibration of the high speed robot Par4 using a laser tracker. *In MMAR'06: 12th International Conference on Methods and Models in Automation and Robotics* (pp. 687-692). IEEE/IFAC.
13. Andreff, N., Renaud, P., Martinet, P., & Pierrot, F. (2004). Vision-based kinematic calibration of an H4 parallel mechanism: practical accuracies. *Industrial Robot: An international journal*, 31(3), 273-283.
14. Renaud, P., Andreff, N., Lavest, J. M., & Dhome, M. (2006). Simplifying the kinematic calibration of parallel mechanisms using vision-based metrology. *IEEE Transactions on robotics*, 22(1), 12-22.
15. Dallej, T., Hadj-Abdelkader, H., Andreff, N., & Martinet, P. (2006, October). Kinematic calibration of a Gough-Stewart platform using an omnidirectional camera. *In Intelligent Robots and Systems, 2006 IEEE/RSJ International Conference on* (pp. 4666-4671). IEEE.
16. Andreff, N., Dallej, T., & Martinet, P. (2007). Image-based visual servoing of a gough—stewart parallel manipulator using leg observations. *The International Journal of Robotics Research*, 26(7), 677-687.
17. Traslosheros, A., Sebastián, J. M., Castillo, E., Roberti, F., & Carelli, R. (2010, October). One camera in hand for kinematic calibration of a parallel robot. *In Intelligent Robots and Systems (IROS), 2010 IEEE/RSJ International Conference on* (pp. 5673-5678). IEEE.
18. Rauf, A., Pervez, A., & Ryu, J. (2006). Experimental results on kinematic calibration of parallel manipulators using a partial pose measurement device. *IEEE Transactions on Robotics*, 22(2), 379-384.
19. Nategh, M. J., & Agheli, M. M. (2009). A total solution to kinematic calibration of hexapod machine tools with a minimum number of measurement configurations and superior accuracies. *International Journal of Machine Tools and Manufacture*, 49(15), 1155-1164.
20. Ren, X. D., Feng, Z. R., & Su, C. P. (2009). A new calibration method for parallel kinematics machine tools using orientation constraint. *International Journal of Machine Tools and Manufacture*, 49(9), 708-721.
21. Abtahi, M., Pendar, H., Alasty, A., & Vossoughi, G. (2010). Experimental kinematic calibration of parallel manipulators using a relative position error measurement system. *Robotics and Computer-Integrated Manufacturing*, 26(6), 799-804.
22. Šika, Z., Hamrle, V., Valášek, M., & Beneš, P. (2012). Calibrability as additional design criterion of parallel kinematic machines. *Mechanism and Machine Theory*, 50, 48-63.
23. Huang, T., Bai, P., Mei, J., & Chetwynd, D. G. (2016). Tolerance Design and Kinematic Calibration of a Four-Degrees-of-Freedom Pick-and-Place Parallel Robot. *Journal of Mechanisms and Robotics*, 8(6), 061018.
24. Wu, J. F., Zhang, R., Wang, R. H., & Yao, Y. X. (2014). A systematic optimization approach for the calibration of parallel kinematics machine tools by a laser tracker. *International Journal of Machine Tools and Manufacture*, 86, 1-11.
25. Li, P., Xie, W., Zhang, X., & Zeng, R. (2017, December). Relative posture-based kinematic calibration of a 6-RSS parallel robot by using a monocular vision system. *In Robotics and Biomimetics (ROBIO), 2017 IEEE International Conference on* (pp. 2567-2572). IEEE.
26. Klimchik, A., Wu, Y., Caro, S., Furet, B., & Pashkevich, A. (2014). Geometric and elastostatic calibration of robotic manipulator using partial pose measurements. *Advanced Robotics*, 28(21), 1419-1429.
27. Joubair, A., Slamani, M., & Bonev, I. A. (2012). A novel XY-Theta precision table and a geometric procedure for its kinematic calibration. *Robotics and Computer-Integrated Manufacturing*, 28(1), 57-65.
28. Shi, H., Su, H. J., Dagalakis, N., & Kramar, J. A. (2013). Kinematic modeling and calibration of a flexure based hexapod nanopositioner. *Precision Engineering*, 37(1), 117-128.

29. Palmieri, G., Palpacelli, M. C., Carbonari, L., & Callegari, M. (2018). Vision-based kinematic calibration of a small-scale spherical parallel kinematic machine. *Robotics and Computer-Integrated Manufacturing*, 49, 162-169.
30. Li, P., Zeng, R., Xie, W., & Zhang, X. (2018). Relative posture-based kinematic calibration of a 6-RSS parallel robot by optical coordinate measurement machine. *International Journal of Advanced Robotic Systems*, 15(2), 1729881418765861.
31. Chen, G., Kong, L., Li, Q., Wang, H., & Lin, Z. (2018). Complete, minimal and continuous error models for the kinematic calibration of parallel manipulators based on POE formula. *Mechanism and Machine Theory*, 121, 844-856.
32. Kong, L., Chen, G., Zhang, Z., & Wang, H. (2018). Kinematic calibration and investigation of the influence of universal joint errors on accuracy improvement for a 3-DOF parallel manipulator. *Robotics and Computer-Integrated Manufacturing*, 49, 388-397.
33. Olarra, A., Allen, J. M., & Axinte, D. A. (2014). Experimental evaluation of a special purpose miniature machine tool with parallel kinematics architecture: Free leg hexapod. *Precision Engineering*, 38(3), 589-604.
34. Olarra, A., Axinte, D., & Kortaberria, G. (2018). Geometrical calibration and uncertainty estimation methodology for a novel self-propelled miniature robotic machine tool. *Robotics and Computer-Integrated Manufacturing*, 49, 204-214.